

Synthesis Effects on the Magnetic and Superconducting Properties of $\text{RuSr}_2\text{GdCu}_2\text{O}_8$

Roberto Masini¹, Cristina Artini², Maria Roberta Cimberle³, Giorgio Andrea Costa², Marilena Carnasciali², and Maurizio Ferretti²

¹ CNR – IENI, Sezione di Milano, Via Cozzi 53, 20125, Milano, Italy

² INFN and DCCI, University of Genoa, Via Dodecaneso 31, 16146 Genoa, Italy

³ CNR – IMEM, Sezione di Genova, Via Dodecaneso 33, 16146 Genoa, Italy

Abstract. A systematic study on the synthesis of the Ru-1212 compound by preparing a series of samples that were annealed at increasing temperatures and then quenched has been performed. It results that the optimal temperature for the annealing lies around 1060-1065 °C; a further temperature increase worsens the phase formation. Structural order is very important and the subsequent grinding and annealing improves it. Even if from the structural point of view the samples appear substantially similar, the physical characterizations highlight great differences both in electrical and magnetic properties related to intrinsic properties of the phase as well as to the connection between the grains as inferred from the resistive and the Curie Weiss behaviour at high temperature as well as in the visibility of ZFC and FC magnetic signals.

1 Introduction

There have been a number of reports on the coexistence of magnetic order and superconductivity in the ruthenocuprate $\text{RuSr}_2\text{GdCu}_2\text{O}_8$, synthesized for the first time in 1995 [1]. Its peculiarity lies in the fact that, unlike previous compounds, magnetic order occurs at a temperature much higher than the superconducting transition temperature. This compound is characterised by a triple perovskitic cell similar to the high temperature superconducting cuprate (HTSC) $\text{YBa}_2\text{Cu}_3\text{O}_x$, in that it contains two CuO_2 layers while the CuO chains are replaced by a RuO_2 layer. However, various experimental reports came to different conclusions. It has been suggested on the basis of transport measurements that its electronic behaviour is similar to an underdoped HTSC [2] while, on the contrary, NMR measurements resulted comparable to those of an optimally doped HTSC [3]. Some other reports concluded that the magnetic order is ferromagnetic in the RuO_2 layers [2,4,5,6] in which case there should be competition between the superconducting and magnetic order parameters resulting eventually in a spontaneous vortex phase formation or spatial modulation of the respective order parameters. However, powder neutron diffraction showed that the low-field magnetic order is predominantly antiferromagnetic [7], with a small ferromagnetic component presumably produced by spin canting. The spectrum of published data includes also non superconducting samples showing similar macroscopic magnetic behaviour [8], samples showing zero resistance but no diamagnetic signal and finally samples with evidence of a resistive and magnetic

transition. Since the physical properties of this rutheno-cuprate material are strongly dependent on the details of the preparation procedure, and can be very different even in samples that turn out to be formally identical to a standard structural and chemical-physical characterization, we have conducted a systematic on the effects of sample preparation conditions on the properties of such hybrid compound.

2 Experimental

The crystal structure was determined by powder X-ray diffraction (XRD) using Cu K_α radiation. Dc resistivity and magnetic measurements were performed by the standard four-probe technique with 1 mA current in a closed-cycle helium cryostat in the temperature range 15 - 300 K and by a Quantum Design SQUID magnetometer respectively. Measurements were performed on similar size bar-shaped sintered polycrystalline specimens allowing comparison of the results.

2.1 Sample preparation

Polycrystalline samples with nominal composition $\text{RuSr}_2\text{GdCu}_2\text{O}_8$ (hereafter referred as Ru-1212) are commonly prepared by solid-state reaction technique from a mixture of high purity RuO_2 (99.95%), Gd_2O_3 (99.99%), CuO (99.9%) and SrCO_3 (99.99%) [1,4,5,9,10,11]. The raw materials are:

- i – first reacted in air at about 960 ° C to decompose SrCO_3 ,
- ii – heated in flowing N_2 at 1010 ° C,
- iii – annealed in flowing O_2 at temperatures ranging from 1050 to 1060 ° C and
- iv - finally, a prolonged anneal in flowing O_2 at 1060 ° C is performed, during which the material densifies, granularity is substantially reduced [12] and ordering within the crystal structure develops [13].

Because the superconducting and magnetic properties are affected by the details of the preparation process, which in turn affect the microscopic structure, a systematic work on the synthesis of Ru-1212 and the effects of sample preparation on the magnetic and superconducting properties was developed [14]. Basically a procedure as described commonly in literature and sketched in Fig.1 has been adopted with the aim to give insight on the formation and stability of the various phases involved in the synthesis of this complex system. Each reaction step was carried out on a MgO single crystal substrate to prevent reaction with the alumina crucible. Between each step the products were thoroughly ground and pressed into pellets.

- i - The stoichiometric oxides were first calcined in air at different temperatures, T_A , for 12 h. XRD spectra performed on these calcined samples are shown in Fig.2 (a), (b), (c). The spectra show the peaks of the Ru-1212 phase whose amount increases with the temperature of the thermal treatment. There are however reflections of second phases identified as SrRuO_3 and Gd_2CuO_4 , with

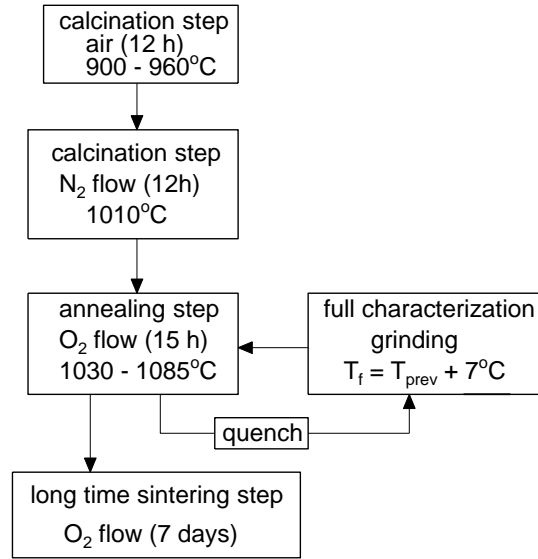


Fig. 1. Sample synthesis and sintering of $\text{RuSr}_2\text{GdCu}_2\text{O}_8$

higher amounts in samples calcined at the lower temperature, diminishing with increasing the calcination temperature.

ii - The pellets were then annealed in flowing nitrogen at 1010°C for 12 h. The sintering in N_2 gas is required to suppress the SrRuO_3 phase [10]. This step resulted in fact in the formation of a mixture of $\text{Sr}_2\text{GdRuO}_6$ and Cu_2O independently of the starting calcined mixture from step (i) (hereafter named L-serie). Typical XRD pattern is shown in Fig.2 (d) obtained from the sample calcined at 900°C which contained the highest amount of SrRuO_3 . No detectable traces, within the resolution of the technique, of such very stable in oxidising environment [10] impurity phase, were observed.

On behalf of these results, the synthesis of Ru-1212 by using SrO_2 as starting reagent in place of SrCO_3 was investigated (sample I). Raw materials were then heated directly in N_2 flow at 1010°C avoiding thus the first calcination step (i) in air. No significant differences were obtained in the composition of the products as inferred from XRD analysis with respect to previous results shown in Fig.2(d).

iii - The L- serie mixture was then subjected to eight successive sintering steps in flowing O_2 , each one lasting 15 h, at successively increasing temperatures in the range $1030^\circ\text{C} - 1085^\circ\text{C}$. Each successive thermal treatment was performed at a temperature about 7°C higher than the previous one. In order to investigate the effects of the thermal treatments the product was quenched to room temperature at the end of every step, fully characterized, reground, pressed into pellets and subjected to the successive thermal treatment.

Powder XRD patterns of all our samples show Ru-1212 as the major phase, with zero to some amount of SrRuO_3 as minor impurity depending on the sample

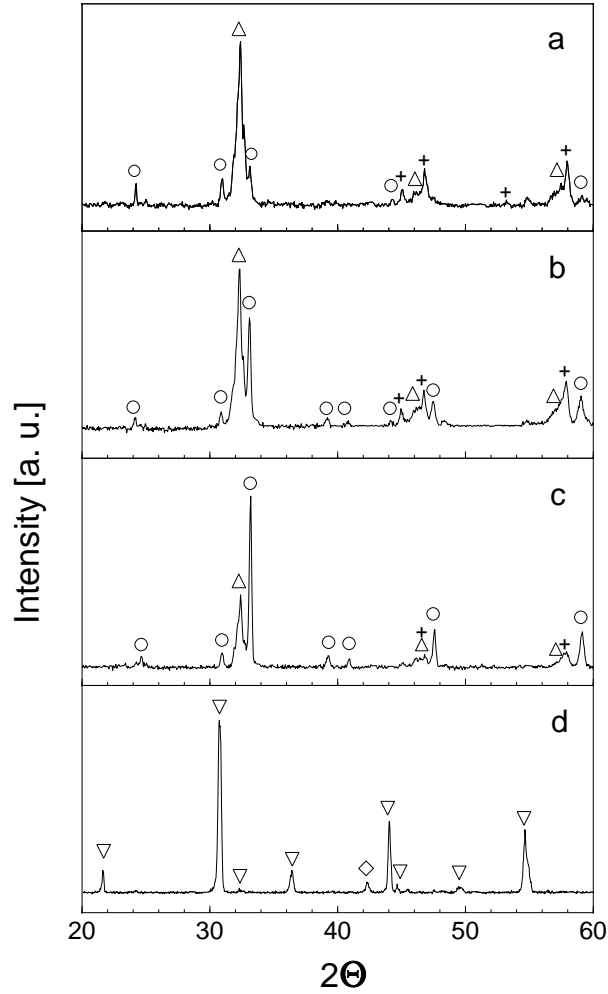


Fig. 2. X-ray spectra for samples calcined at (a) $T_A = 900$, (b) 940 and (c) 960 °C in air for 12h. \circ Ru-1212, \triangle SrRuO₃ and $+$ Gd₂CuO₄; (d) after annealing in N₂ for 15h ∇ Sr₂GdRuO₆, \diamond Cu₂O

preparation condition. Traces of second phase SrRuO₃ (2% vol. for sample L1) with decreasing amount up to sample L3 were detected. Single phase materials were obtained afterwards. All peaks can be indexed assuming a tetragonal lattice and Table 1 lists the lattice parameters calculated for these Ru-1212 samples. In Fig.3 the X-ray powder diffraction pattern of sample L5, synthesized after five sintering steps up to 1067 °C for a total time $t = (15 \times 5) = 75$ h, is reported.

The same XRD spectra have been obtained for sample I, subjected to a subsequent thermal treatment at 1050 °C for 24 h and successively to a prolonged anneal at 1060 °C for a week in O₂ flow.

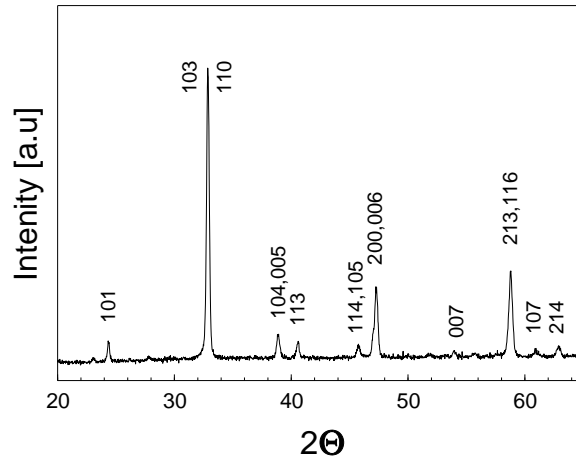


Fig. 3. XRD pattern of sample L5

Table 1. Synthesis, structural and electrical data of L-series Ru-1212 samples

sample	T_{ann} (°C)	a (Å)	c (Å)	ρ_{290} ($m\Omega\text{cm}$)	$T_{R=0}$ (K)	T_{max} (K)
L1	1031	3.826(2)	11.516(7)	154.8	— ^a	37
L2	1037	3.821(3)	11.528(8)	141.7	— ^a	44
L3	1044	3.831(1)	11.545(7)	140.9	— ^a	46
L4	1053	3.831(1)	11.547(6)	70.6	17	48
L5	1061	3.828(1)	11.552(6)	30.6	25	49
L6	1067	3.844(1)	11.585(3)	14.0	21	44
L7	1073	3.845(1)	11.610(5)	23.7	21	47
L8	1084	3.835(1)	11.580(5)	22.0	— ^a	45

^a No information available below 15 K. See text for a complete discussion.

Parallel checks have been performed allowing us to conclude that reaching the “optimal” temperature directly in one step for a time which is the sum of the corresponding partial times of each single step covered up to the same temperature does not produce the same results of the longer procedure described above. Single-phase formation seems to be kinetically hindered by the slow decomposition rate of the impurities which already formed upon calcination. Repeated homogenisations, related to the sequence of grinding and annealing, improve the phase purity of the material and control the superconducting behaviour.

Morphologically, all the L-series samples show a high grain homogeneity with clean grain boundaries as probed by SEM and microprobe analyses. Fig.4 shows

the typical granular morphology detectable at the beginning of the thermal treatment cycles (sample L2) with an average grain size of about $2\ \mu\text{m}$.

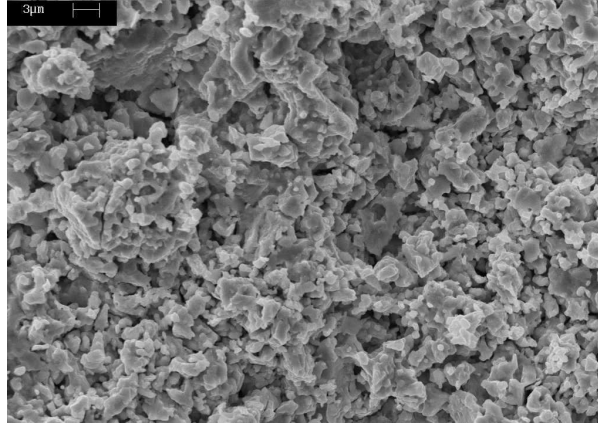


Fig. 4. SEM picture of sample L2

A progressive grain growth and a corresponding increase in grain connectivity due to the different thermal treatments can be observed (Fig.5, sample L6, it can be noticed how some grains begin to coalesce into big aggregates dispersed in an almost unchanged granular matrix), without reaching, by the way, complete sintering at the highest temperature.

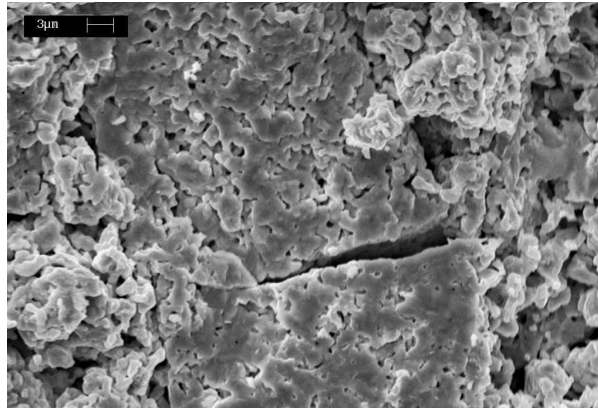


Fig. 5. SEM picture of sample L6

Such behaviour is related to the difference between the decomposition temperature of the 1212 phase and the maximum temperature of the thermal processes considered in this work.

A geometric density variation of about 5% between the first and the final bulk sample has been measured ($d \approx 4.2 \text{ g/cm}^3$ corresponding to about 63% of the theoretical crystallographic density).

3 Electrical properties

In general resistivity measurements of Ru-1212 show a superconducting transition at 45 K with a very slight upturn in the vicinity of T_c reaching zero resistivity at a lower temperature between 20 – 30 K. The resistivity transitions at $H = 0$ are much broader than those observed in many of the other HTSC. A metallic behaviour, with a T linear dependence at high temperatures above 100 K, is usually observed. A magnetic transition at $T_M = 132 \text{ K}$ manifest itself as a small yet noticeable kink/minimum in the resistivity related to the onset of the magnetic ordering of the Ru lattice.

Since the oxygen stoichiometry is practically unchanged in Ru-1212, the annealing turns out to influence mainly the granularity and ordering within the crystal structure. Previous studies have shown that the semiconductor-like upturn and the zero resistivity temperature are critically dependent on the sample processing. [10,15]. In particular, according to [6] the slight upturn in the vicinity of T_c is related to grain boundary effects. High resolution TEM study on Ru-1212 has shown that prolonged thermal treatment at 1060°C in O_2 removes most of a multidomain structure, consisting predominantly of 90° rotations, as well as significantly reduces the semiconductor-like upturn [15]. Part of the superconducting transition width may be due to structural disorder. However it must be underlined that a broad superconducting transition is also expected within the spontaneous vortex phase model [16].

Curves of $\rho(T)$ of selected samples (L-serie) considered significative, for sake of clarity, of the overall process of synthesis are shown in Fig.6. All samples exhibit weakly pronounced or local minima in the dc resistivity near the magnetic transition temperature, of the order of about 132 K. This feature is more clearly visible in the inset of the figure where the derivative of the resistivity (sample L4) is plotted.

At low temperatures the dc resistance shows a semiconductor-like upturn followed by a sudden decrease in resistivity starting at T_{max} and achieving zero resistivity state for temperatures below 30 K as reported in Table 1. There is a small increase in the zero resistivity temperature for our best sample (L6) and only a small reduction in the semiconductor-like upturn. Summarizing the general trend, it can be stated that the resistivity is progressively decreased and a crossover from a semiconducting to metallic normal state resistivity behaviour is observed on going from L1 to L8 sample. We underline that zero resistivity has not been reached for samples from L1, L2, L3 and L8 even if, considering their strong resistivity drop detected below 45 K, a $R = 0$ value is expected at a temperature lower than 13 K for samples L2, L3 and L8. A comparison between the resistivity behaviours, independently of their granular nature, has

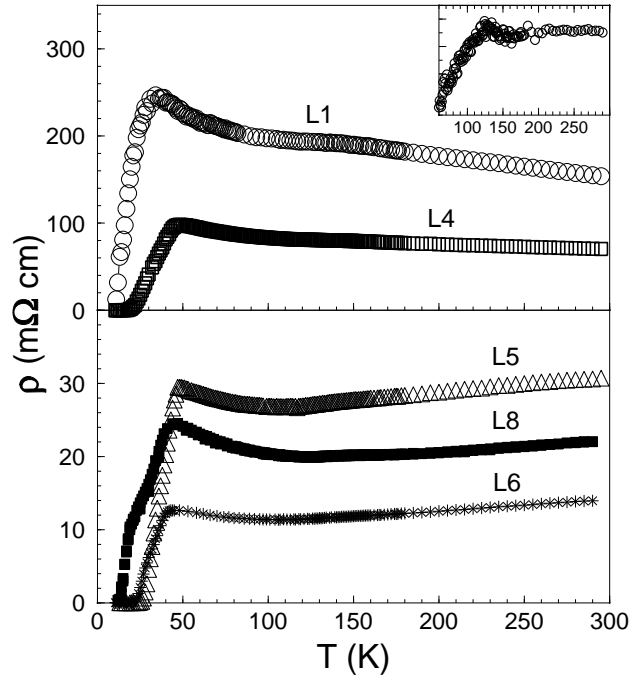


Fig. 6. Resistivity vs T curves of some selected L-series samples synthesized under different conditions. Inset: $d\rho/dT$ temperature dependence for sample L4 around T_M

been possible because different values are not related to the sample density variations, which as already noted is almost unchanged for all the samples.

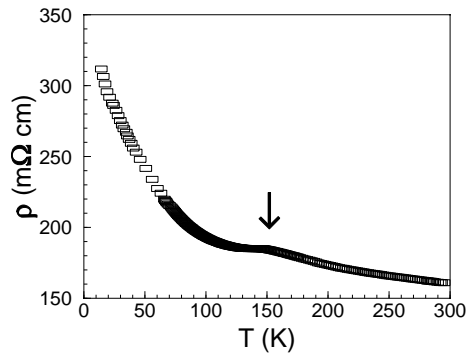


Fig. 7. Resistivity temperature dependence of sample I

A semiconducting-like transport with no indications of transition to superconductivity at low temperatures is observed for sample E in all the temperature range considered, as shown in Fig. 7. It is noteworthy that a kink in resistivity

is observed in the vicinity of T_M (arrow in Fig. 7). This anomaly is due to a reduction of spin scattering. Such a behaviour is also observed in SrRuO_3 single crystals [17] at around its ferromagnetic transition temperature.

The derivative of resistivity, shown in Fig. 8 for L3 – L8 samples, clearly shows two overlapping maxima, indicating that the resistive transition proceeds in two steps: a high temperature contribution, associated with the thermodynamic superconducting transition temperature and another one, at a lower temperature, which critically depends on sample processing conditions [10,14,15] as well as the zero resistance temperature value.

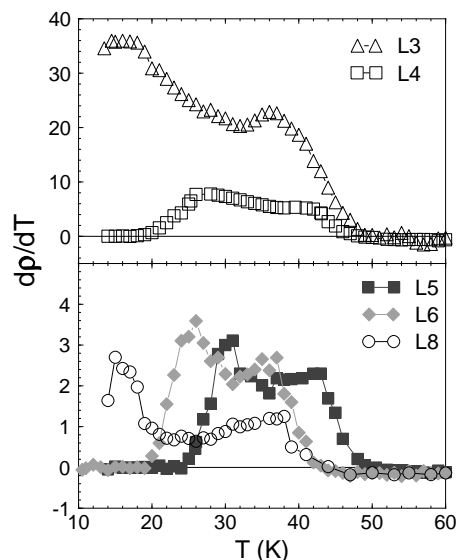


Fig. 8. $d\rho/dT$ temperature dependence

Since from the analysis of x-ray patterns our superconducting and non superconducting samples are indistinguishable, more insight about the physical nature of the superconducting and magnetic states is expected from magnetic measurements.

4 Magnetic properties

The magnetic characterization of the ruthenocuprate materials is a crucial and not trivial point. Magnetic measurements are obviously a key tool to observe both the superconducting and magnetic behaviour of these samples, but many years after their successful synthesis [1] and in spite of a great experimental effort devoted to this problem, many doubts still survive about the magnetic ordering present in these type of samples [7, 11, 18, 19, 20, 21, 22].

First of all, we recall that generally granular samples are measured: therefore, all the problems related to the granular behaviour of HTSC and, in general, to the distinction between intrinsic and extrinsic properties (intra-granular and inter-granular) must be born in mind.

A first problem encountered in the observation of the superconducting behaviour is the fact that the standard diamagnetic signals, both in the Field Cooled (FC) and Zero Field Cooled (ZFC) mode, are not always seen in all the samples of such compounds [13, 14, 18, 23]: what is more often observed is the shielding signal, rarely the diamagnetism related to the FC procedure. Both signals are quickly removed by the application of even a small external magnetic field (few tens of Gauss). In contrast, even when in the magnetic measurement there is no trace of superconducting behaviour, it may be observed resistively and the application of even a high external magnetic field (up to Tesla) does not destroy it [24]. The reason for such a contradictory phenomenology may be understood bearing in mind the simultaneous presence of magnetic and superconducting ordering in these samples. This fact implies consequences both on the sample physical behaviour and on the measurement technique used to monitor it. We recall that μ SR measurements [5] indicate the homogeneous presence of an internal field that, at low temperature, may reach hundreds of Gauss and may give rise to a spontaneous vortex phase (SVP) in the temperature range where it exceeds the first critical field $H_{c1}(T)$ [25]. In a type II superconductor at $H > H_{c1}$ the Meissner effect is practically never observed for the presence inside the materials of “pinning centres” that are able to block the flux lines and prevent their expulsion. This is the reason why the FC diamagnetic signal may be very small and its difference from the ZFC signal is an indication of the critical current density that a sample can carry. A vast literature related to high T_c superconductors illustrates unambiguously this item [26, 27]. Moreover, as noted in [28], the magnetization of ruthenocuprate materials contains magnetic signals arising from different contributions: the Gd paramagnetic spin lattice, the Ru spin lattice and, finally, the diamagnetic signal related to the superconducting behaviour. Both for Gd and Ru spin lattice the antiferromagnetic ordering is coupled with a ferromagnetic component that, in the case of Ru, is attributed to a canting of the lattice and in the case of Gd is simply related to the presence of the net ferromagnetic moment of the Ru lattice [20]. The simultaneous presence of such opposite magnetic signals makes the magnetic measurement unsuitable for the observation of the superconductivity: in fact, such measurement cannot separate the magnetic signal related to superconductivity from that related to the magnetic ordering. Moreover, it is clear that the application of an external magnetic field exalts the magnetic signals and depresses the superconducting one, destroying very quickly the visibility of the superconductivity. In the light of these considerations we can understand the fact that the superconducting behaviour is often observed resistively but not magnetically: it depends on the competition between two opposite magnetic signals, one related to the magnetic ordering, the other to the superconducting one. “More superconductivity” is obviously related to many factors: the amount of

superconducting phase inside the sample, the quality of the connection between the grain that makes the shielded volume and therefore the related magnetic signal smaller or larger, and the intrinsic properties of the Ru-1212 phase that, as we will see, may change in connection with the grade of order of the material. Now, dealing with the experimental problems, we point out the following. In order to enhance the superconducting behaviour it is suitable to apply magnetic fields as small as possible. This fact, due the peculiar modalities of elaboration of the instrumentation commonly used, must be considered in detail. The first problem is the exact knowledge of the field that is effectively seen by the sample, and the second is strictly related to the complexity of the magnetic signal present in these samples. A small remanent magnetic field in the superconducting coil of the experimental set-up is often present. It may be zeroed by a procedure that, starting from a value of some Tesla, applies coercive fields of decreasing intensity. In such a way the field is zeroed but for a few Gauss that may be zeroed in the central point of the magnet by applying a small counterfield. Anyway, a very small residual field survives and turns out to be of the order of fractions of Gauss. In the light of what has been said, a real ZFC measurement cannot be made and, since the FC magnetic moment is about one order of magnitude greater than the ZFC, also a residual field of fractions of Gauss may give a considerable magnetic signal whose polarity depends on the field polarity. In addition, the basic condition of a homogeneous magnetic moment required by the SQUID magnetometer is not fulfilled, in particular at low temperatures, where, as a consequence of the applied field, magnetic moments of opposite polarity will be present in the sample. Finally, we recall that during the measurements the sample is moved for a length that is usually of few centimetres, so that it travels in a non uniform magnetic field that makes it follow a minor hysteresis loop. If the value of the moment is not constant during the scan, an asymmetric scan wave form will be observed and the quality of the measurement will drastically degrade [29].

All we have said is illustrated in Fig. 9 where magnetization measurements are reported for both ZFC and FC conditions. For sake of clarity we report data for some representative samples only. The cuspid at $T \cong 30$ K marks the magnetic ordering: there is a small variation in this temperature, which is smaller in the sample with higher superconducting temperature in agreement with the literature data [8]. It is remarkable to observe the different behaviour exhibited by the various samples: L3 gives no hint of superconductivity, L5 exhibits a very clear shielding corresponding to about 75% of the maximum diamagnetic signal at $\mu H_{\text{ext}} = 0.5$ G while at $\mu H_{\text{ext}} = 5$ G its transition is strongly worsened, L6 shows a diamagnetic shift after an ascent of the magnetization (probably due to the instrumental effects we outlined before, for the presence of two opposite magnetic signals of similar magnitude), and L8 shows a behaviour very similar to L3. At the lowest temperatures a large contribution from Gd sublattice, which orders antiferromagnetically at 2.5 K, is clearly visible in FC magnetization curves for the magnetically non superconducting samples L3 and L8. If the superconductivity is marked by the visibility of a diamagnetic shift of the ZFC

or FC signals, such behaviour is surely absent in L1, L2, L3, L4 and L8 while, to different extent, it is observed in L5, L6 and L7. In the resistivity measurements, on the contrary, all the samples show a large drop of resistivity, but at the temperature of $T=13$ K (the minimum value at which we measured resistively, while magnetically we reached $T=5$ K) zero is reached for L4, L5, L6 and L7 samples.

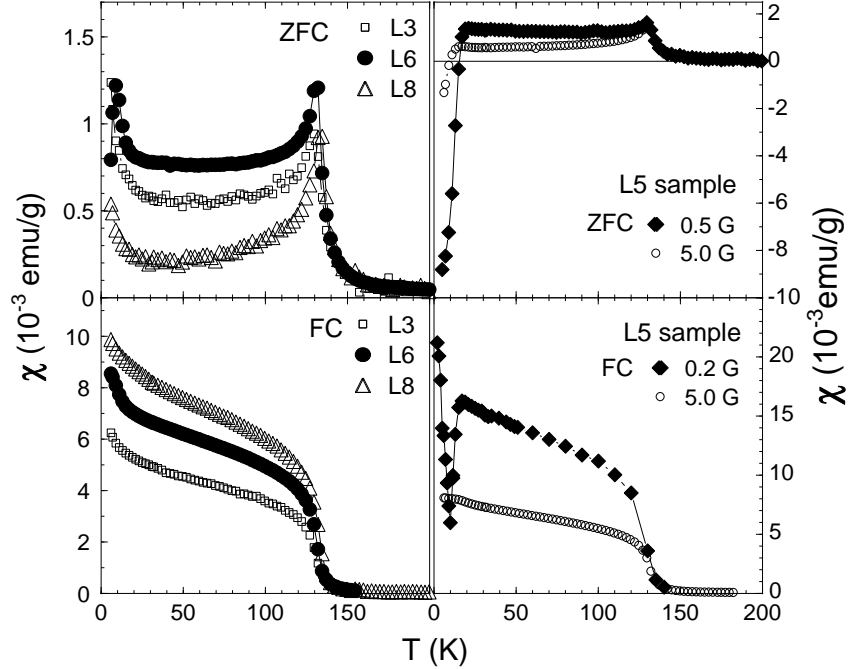


Fig. 9. ZFC and FC susceptibility vs temperature curves for some samples of the L-series: *left* L3 (5.5 G), L6 (5.5 G) and L8 (3.0 G); *right* L5 sample

In lower Fig. 9 the FC data for samples L3, L5, L6 and L8 are shown. A sudden onset of a spontaneous magnetic moment appears, related to a ferromagnetic component arising from Ru spin ordering in RuO_2 planes. Such a spontaneous magnetization develops at a temperature in the 130-135 K range and below 110 K it rises almost linearly as temperature decreases down to about 50 K. We remark the very similar behaviour of L3 and L8, already observed in upper part of Fig. 9. A clear diamagnetic behaviour is seen only in L5: at the minimum applied field of 0.2 G, and to a minimum extent even at 1.2 G, a diamagnetic behaviour that quickly reenters is seen in the FC curve. At 5.5 G the diamagnetic effect is only seen as a constant value hindering the Gd magnetic ordering. Such behaviour has been already observed [30].

In Fig. 10 we present the inverse of ruthenium susceptibility as a function of temperature for all the samples in the series L1-L8. In the calculation of the

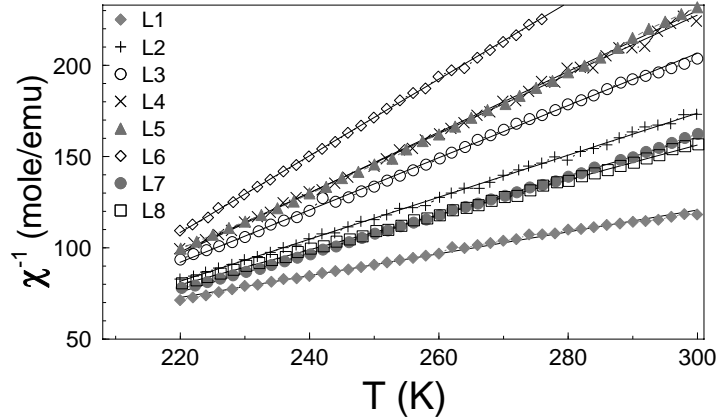


Fig. 10. χ_{Ru}^{-1} vs temperature for all the samples. Fitting results are shown as solid lines

ruthenium susceptibility we have followed the procedure suggested by Butera et al. [22]. Such a procedure calculates the Ru susceptibility by subtracting three magnetic contributions to the experimental value: 1) the paramagnetic contribution from Gd ions, 2) the core diamagnetism for the 1212 compounds as deduced from the Landolt-Börnstein tables, and 3) a temperature-independent Pauli-like contribution coming from the conduction electrons. The so obtained ruthenium susceptibility is fitted by the Curie-Weiss relationship $\chi_{\text{Ru}} = \frac{C_{\text{Ru}}}{(T-\Theta)}$ and allows to calculate both the Curie temperature Θ and the effective magnetic moment μ_{eff} for Ru atom. Although a maximum content of about 2 vol.% of SrRuO_3 impurity phase was detected from x-ray analyses in sample L1, with decreasing amount to zero for sample L4, a similar negligible error on the absolute values of $\mu_{\text{eff}}^{\text{Ru}}$ and θ has been calculated with no significant effect on their general behaviour.

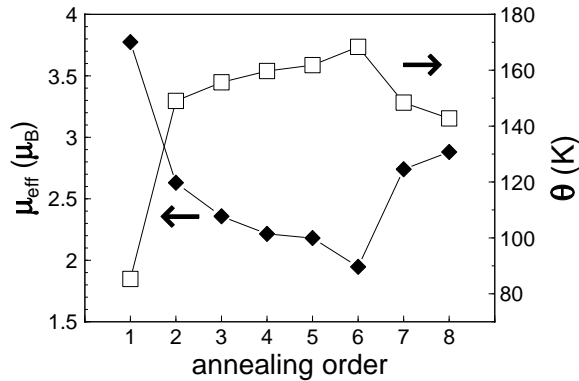


Fig. 11. $\mu_{\text{eff}}^{\text{Ru}}$ and θ calculated from a best fit of χ_{Ru}^{-1} vs temperature data

The obtained results are reported in Fig. 11 and in Table 2 as a function of the number of annealing steps that give rise to the sequence L1-L8.

Table 2. $\mu_{\text{eff}}^{\text{Ru}}$ and θ values as a function of annealing steps and “superconductivity” status of all L-series samples

sample	$\mu_{\text{eff}}^{\text{Ru}}(\mu_B)$	$\theta(\text{K})$	res ^a	m_{ZFC}^a	m_{FC}^a
L1	3.77	85.3	– ^b	no	no
L2	2.63	149.0	– ^b	no	no
L3	2.36	155.6	– ^b	no	no
L4	2.21	159.7	yes	no	no
L5	2.18	161.8	yes	yes	yes
L6	1.95	168.3	yes	yes	yes
L7	2.74	148.4	yes	yes	no
L8	2.88	142.7	– ^b	no	no

^a measurement technique utilized to detect superconductivity: resistivity, ZFC and FC magnetization.

^b No information available below 15 K. See text for a complete discussion.

Starting from L1 the Θ values increase, reach a maximum (around L5-L6 of about 160 K), and then decrease going up to L8. The μ_{eff} values have a specular trend, decreasing from the value 3 for L1 down to a minimum value of about 2 at L6, and then slightly increasing once again. Since the superconductivity is better observed in the samples L5, L6, L7 both by resistivity and magnetic measurements, these data suggest that an improved superconducting behaviour may be related to small intrinsic variations in the structure of the sample that produces smaller effective magnetic moments for Ru atom and higher Curie temperatures. We give here only some suggestions to be explored. The μ_{eff} values derived by the best fit imply that Ru is in a mixed valence state between Ru^{4+} and Ru^{5+} . Such a result has been firstly proposed by Liu et al. [21] through XANES spectroscopy and successively confirmed by Butera et al. [22] through magnetic measurements by means of the procedure we have outlined. These results definitively contradict the hypothesis that Ru exhibits an effective moment $\mu_{\text{eff}} \cong 1 \mu_B/\text{Ru atom}$, as proposed in [4]. On passing from L1 up to L8 the proportion of Ru^{4+} and Ru^{5+} changes. Possible consequences of this fact are: slight variations in the carriers number and, as a consequence, in the critical temperature (see the resistivity data in Fig.6 and Table 1), different coupling between the superconducting and the magnetic planes both in term of total magnetic moment seen by the conduction electron (with increased or decreased pair-breaking effect) and in term of coupling between orbitals of superconducting and magnetic electrons [31]. The origin of these variations may be found in a different degree

of lattice disorder following the various annealing steps performed at different temperatures that, as we have widely observed, produce significant variations in all the physical properties. Moreover, the lattice disorder can imply a certain amount of Cu \rightarrow Ru substitutions that are a possible candidate for the observed variations of the effective magnetic moment. Also the variation of Θ may be the consequence of the different coupling between Ru atoms following the different valence state.

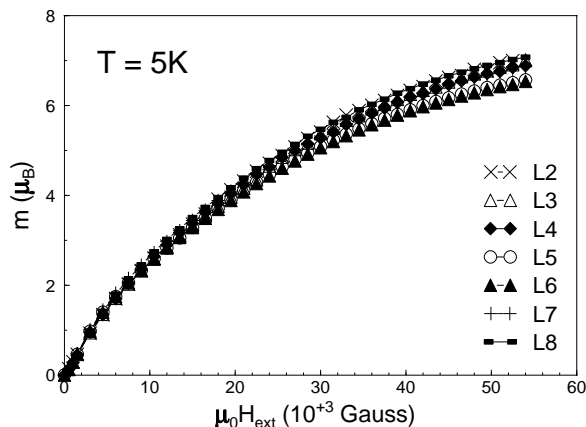


Fig. 12. Magnetic moment versus magnetic field at 5K for L-series samples

The same trend we have seen in μ_{eff} is observed in the saturation moment as seen by measuring magnetization up to the maximum field of 5.5 Tesla at T=5 K. Results are shown in Fig 12. The values change from the minimum value of $6.5 \mu_B$ for L5 and L6 samples up to a maximum value of $7 \mu_B$ in the L2 and L8 samples. We remark that in the experimental conditions we have used the saturation is not completely reached, but the hierarchy of the saturated magnetic moments is surely correct.

5 Conclusions

The magnetic and superconducting properties of Ru-1212 have been studied and compared for a series of samples synthesized under different conditions with the aim to find out the fundamental parameters ruling out the phase formation and its related structural and physical properties. From our experimental work it results that the optimal annealing temperature lies in a narrow temperature range around 1060-1065 °C; further temperature increase worsens the phase formation. Subsequent grinding and annealing steps up to this temperature improve the phase homogeneity. A wide range of physical properties has been obtained on quenched samples from the same batch, which differ only in the synthesis procedure parameters. No other substantial differences were detected

for these samples, all showing similar compositional and structural characteristics. It emerges that the preparation method plays an important role when dealing with the magnetic and superconducting properties of this hybrid compound. So far, published data on the Ru-1212 phase show the same general trend for what regards the measured physical properties. Because most of the samples are chemically and structurally comparable, great care must be taken in the preparation process details such as the final sintering temperature and the number of homogeneity steps (if any) performed up to that temperature. Only samples with the same thermal history/parameters can be compared.

References

1. L. Bauernfeind, W. Widder, H.F. Braun: *Physica C* **254**, 151 (1995)
2. J.L. Tallon, J. W. Loram, G.W.M. Williams, C. Bernhard: *Phys. Rev. B* **61**, 6471 (2000)
3. Y. Tounaga, H. Kotegawa, K. Ishida, Y. Kitaoka, H. Takigawa, J. Akimitsu: *Phys. Rev. Lett.* **86**, 5767 (2001)
4. C. Bernhard, J.L. Tallon, Ch. Niedermayer, Th. Blasius, A. Golnik, E. Brücher, R.K. Kremer, D.R. Noakes, C.E. Stronach, E.J. Ansaldo: *Phys. Rev. B* **59**, 14099 (1999)
5. J. Tallon, C. Bernhard, M. Bowden, P. Gilberd, T. Stoto, D. Pringle: *IEEE Trans. Appl. Supercond.* **9**, 1696 (1999)
6. J.E. McCrone, J.R. Cooper, J.L. Tallon: *J. Low Temp. Phys.* **117**, 1199 (1999)
7. J.W. Lynn, B. Keimer, C. Ulrich, C. Bernhard, J.L. Tallon: *Phys. Rev. B* **61**, 14964 (2000)
8. R.W. Henn, H. Friedrich, V.P.S. Awana, E. Gmelin: *Physica C* **341-348**, 457 (2000)
9. C.W. Chu, Y.Y. Xue, R.L. Meng, J. Cmaidalka, L.M. Dezaneti, Y.S. Wang, B. Lorenz, A.K. Heilman: *cond-mat* 9910056
10. L. Bauernfeind, W. Widder, H.F. Braun: *J. Low Temp. Phys.* **105**, 1605 (1996)
11. O. Chmaissem, J. D. Jorgensen, H. Shaked, P. Dollar, J. L. Tallon: *Phys. Rev. B* **61**, 6401 (2000)
12. G.V.M. Williams, M. Ryan: *Phys. Rev. B* **64**, 94515 (2001)
13. P.W. Klamut, B. Dabrowski, M. Maxwell, J. Mais, O. Chmaissem, R. Kruk, R. Kmieciak, C.W. Kimball: *Physica C* **341-348**, 455 (2000)
14. C. Artini, M.M. Carnasciali, G.A. Costa, M. Ferretti, M.R. Cimberle, M. Putti, R. Masini: *Physica C* (2002) in press
15. A.C. McLaughlin, W. Zhou, J.P. Attfield, A.N. Fitch, J.L. Tallon: *Phys. Rev. B* **60**, 7512 (1999)
16. C. Bernhard, J.L. Tallon, E. Brücher, R.K. Kremer: *Phys. Rev. B* **61**, 14960 (2000)
17. M. Shepard, G. Cao, S. McCall, F. Freibert, J.E. Crow: *J. Appl. Phys.* **79**, 4821 (1996)
18. C.W. Chu, Y.Y. Xue, S. Tsui, J. Cmaidalka, A.K. Heilman, B. Lorenz, R.L. Meng: *Physica C* **335**, 231 (2000)
19. G.V.M. Williams, S. Kramer: *Phys. Rev. B* **62**, 4132 (2000)
20. J.D. Jorgensen, O. Chmaissem, H. Shaked, S. Short, P.W. Klamut, B. Dabrowski, J.L. Tallon: *Phys. Rev. B* **63**, 54440 (2001)
21. R.S. Liu, L.Y. Jang, H.H. Hung, L.L. Tallon: *Phys. Rev. B* **63**, 212507 (2001)

22. A. Butera, A. Fainstein, E. Winkler, J. Tallon: Phys. Rev. B **63**, 054442 (2001)
23. H. Srikanth, L. Spinu, T. Kodankandath, J.B. Wiley, J. Tallon: J. Appl. Phys. **89**, 7487 (2001)
24. P.W. Klamut, B. Dabrowsky, S. Kolesnik, M. Maxwell, J. Mais: Phys. Rev. B **63**, 224512 (2001)
25. E.B. Sonin, I. Felner: Phys. Rev. B **57**, R14000 (1998)
26. M. Murakami: 'Flux pinning of melt processed YBCO superconductors and their applications'. In: *Studies of High Temperature Superconductors Vol.9.* ed A. Narlikar (Nova Science Publisher, New York 1992) pp. 1-36
27. M. Murakami: *Melt Processed High-Temperature Superconductors* (World Scientific, Singapore 1992)
28. I. Felner, U. Asaf, Y. Levi, O. Millo: Phys. Rev. B **55**, R3374 (1997)
29. M. Suenaga, D.O. Welch, R. Budhani: Supercond. Sci. Technol. **5**, S1 (1992)
30. B. Lorenz, R.L. Meng, J. Cmaidalka, Y.S. Wang, J. Lenzi, Y.Y. Xue, C.W. Chu: Physica C **363**, 251 (2001)
31. A.B. Shick, R. Weht, W.E. Pickett, J. Supercond. **13**, 687 (2000)